A vane pump integrated with an electric motor

Conference Paper · March 2014

READS
26

4 authors, including:

Wieslaw Fiebig
Wroclaw University of Science and Technol…
30 PUBLICATIONS **15** CITATIONS
SEE PROFILE

Ignacy Dudzikowski
Wroclaw University of Science and Technol…
28 PUBLICATIONS **38** CITATIONS
SEE PROFILE

Marek Ciurys
Wroclaw University of Science and Technol…
21 PUBLICATIONS **18** CITATIONS
SEE PROFILE

A vane pump integrated with an electric motor

Wieslaw Fiebig*, Dudzikowski Ignacy**, Ciurys Marek**, Kuczwara Hubert*

Wroclaw University of Technology, Institute of Machine Design*, Institute of Electrical Machines, Drives and Measurements**, Wybrzeze Wyspianskiego 27, 51-370 Wroclaw, Poland
E-Mail: wieslaw.fiebig@pwr.wroc.pl, ignacy.dudzikowski@pwr.wroc.pl, marek.ciurys@pwr.wroc.pl, hubert.kuczwara@gmail.com

In this paper an innovative design solution of a vane pump integrated with an electric motor is presented. An integrated motor-pump assembly with a supply converter and control system has been developed and electromechanical and hydraulic processes in the motor pump group are analyzed. A simulation model of the motor pump group has been developed in order to investigate its functionality, electromechanical and hydraulic parameters and dynamics of the system.

Keywords: vane pumps, electric motors, control systems, integrated motor pump group, fluid power drives
Target audience: Displacement Units, New Approaches and Methods, Simulation

1 Introduction

In most fluid power drives the connection between the pump and electric motor is realized through an elastic clutch and a mounting flange. The pumps are usually driven with electric motors at constant speed /1/. There are solutions in which the pumps are driven with an asynchronous electric motor with a frequency transformer for the rpm control, but these solutions are relatively seldom in application due to their weak dynamic properties. The possibility to control the flow of the displacement pumps directly through the rotational speed has many advantages and is an important simplification of fluid power drives. The proposed solution is based on the concept of using the variable speed electric drive and hydraulic pump with constant displacement. The control systems with the rotational speed control have higher efficiency, due to the adjustment of the power of the electric motor to the power required from actuators (hydraulic cylinder or hydraulic motor).

2 Design principle

In the proposed solution (Figure 1) the hydraulic pump is built into the rotor of electric motor with permanent magnets (BLDC). The rotor of the electric motor causes the rotation of the pump housing. The internal part of the pump with the vanes is not movable. Due to lack of rotation the vanes are pressed to a cam ring with spring elements. The results presented in this paper consider the double vane pump. An example of a similar solution is the pump EPAI from the Voith company /2/.

Double vane pumps have a lot of advantages, such as, load compensation, small reaction forces in the bearings ,and relatively high efficiency. The double vane pumps have maximal pressures up to 200 bar and rotational speed from 500 to 4000 rpm . These pumps are also often applied due to their high durability and simple design and manufacturing /3/.

Figure 1 shows a cross-section of a double-acting vane pump integrated in the rotor of a Brushless Direct Current electric motor with permanent magnets (BLDC motor). A Brushless Direct Current motor has been used, because such motors have the highest energy efficiency, the highest power value per unit mass, large durability and very good dynamic range.

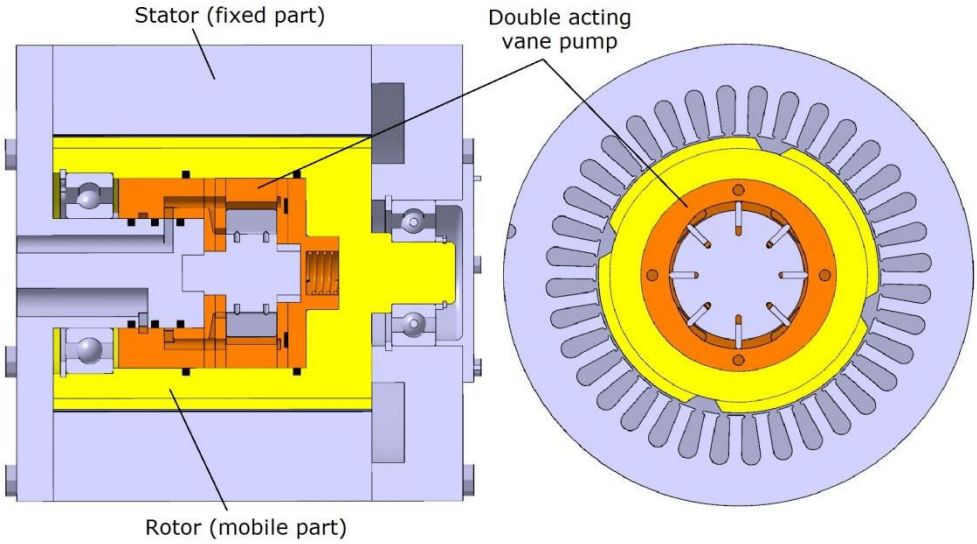

Figure 1: The double vane pump integrated with the BLDC electric motor.

The proposed solution is about 40% smaller in volume than the conventional one with the separate pump and motor. The complete variable rotational speed drive system in that configuration consists of the following elements:

- electrical motor with the permanent magnets (PMM),

- supply converter,

- control system.

3 Modelling of pressure and dynamic torque in the double vane pump Design principle

During the rotation of the pump against the non-rotating part inner pressure changes occur due to compression and decompression of the fluid as well as due to the leakages in the gaps inside the pump. The first step of the calculation of the flow and pressure changes is to identify changes of the volume of the chamber between the vanes.

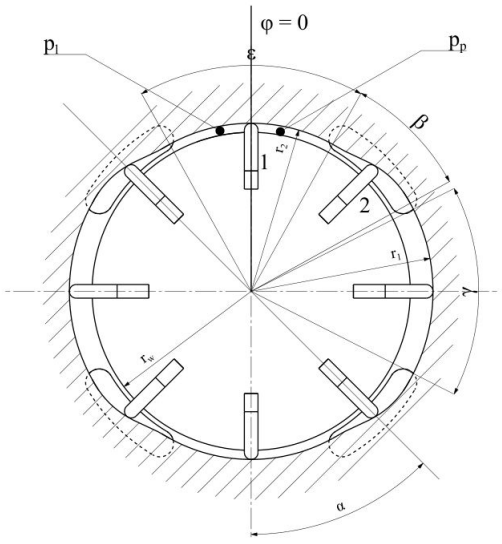

Figure 2: A schematic view of the double vane pump.

The starting position of the rotational angle φ is labelled as 0 in the Figure 2. The change of the cam ring radius during rotation is described on the basis of vane No. 1. The radius is constant and equal r_2 up to angle position φ= ε/2. For the angle range ε/2 < φ< β the radius can be calculated from /3/:

$$\rho(\phi) = r_2 + \frac{r_1 - r_2}{\beta}\phi - \frac{r_1 - r_2}{2\pi}\sin\left(\frac{2\pi}{\beta}\phi\right), \text{ where} \tag{1}$$

ϕ = φ – ε/2 , ε/2 < φ < ε/2 +β

In the angle range ε/2 + β < φ < ε the radius is r_1 . If φ > 3/2·ε + β the radius can be calculated from eq. (1) with ϕ = 3/2·ε + 2β - φ. After the angle position is in the range 3/2·ε + β < φ <180 the radius is constant and equal r_2.

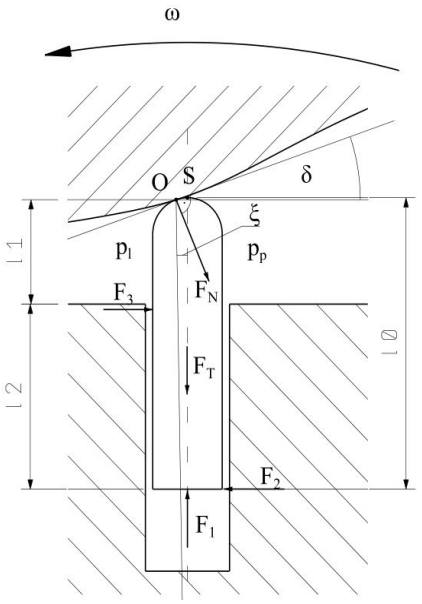

F_T – the friction force in the axial gap

F_1 – force from supporting pressure and springs

F_2, F_3, F_N – reaction forces

Figure 3: A schematic view of the forces acting on the vane.

The angle δ is determined by the first derivative at the contact point on the transition curve:

$$\delta = arc\tan\left[\frac{1}{\rho}\cdot\frac{\partial\rho}{\partial\phi}\right], \text{ where:} \tag{2}$$

$$\frac{\partial\rho}{\partial\phi} = \frac{r_1 - r_2}{\beta} - \frac{r_1 - r_2}{\beta}\cdot\cos\left(\frac{2\pi}{\beta}\cdot\phi\right) = \frac{r_1 - r_2}{\beta}\cdot\left[1 - \cos\left(\frac{2\pi}{\beta}\cdot\phi\right)\right] \tag{3}$$

The point O is the contact point of the vane with the internal surface of the cam ring and its position is different from the middle point on the top of the vane The position of the contact point between the vane and cam ring is approximated from:

$$\xi = \frac{s/2}{\rho}\cdot\sin\delta \tag{4}$$

Finally the radius of the contact point O is equal to the radius by the angle φ-ξ.

The radius at the top of the vane (S) is greater than or equal to the radius of the contact point and depends on the angle δ, as follows:

$$r_v(\varphi) = \rho(\varphi - \xi) + \frac{s}{2} \cdot (1 - \cos\delta) \tag{5}$$

Length l_1 and l_2 can be calculated from /3/:

$$l_1(\varphi) = \rho(\varphi - \xi) - r_w \tag{6}$$

$$l_2(\varphi) = l_0 - (r - r_w) \tag{7}$$

The speed and acceleration of vanes in radial direction can be calculated from:

$$\dot{y} = \frac{\partial \rho}{\partial t} = \frac{r_1 - r_2}{\beta} \cdot \dot{\varphi} - \frac{r_1 - r_2}{\beta} \cdot \dot{\varphi} \cos\left(\frac{2\pi}{\beta} \cdot \phi\right) \tag{8}$$

$$\begin{aligned} \ddot{y} &= \frac{\partial^2 \rho}{\partial t^2} = \frac{r_1 - r_2}{\beta} \cdot \ddot{\varphi} - \frac{r_1 - r_2}{\beta} \cdot \ddot{\varphi} \cos\left(\frac{2\pi}{\beta} \cdot \phi\right) + 2\pi \cdot \dot{\varphi}^2 \cdot \frac{r_1 - r_2}{\beta^2} \cdot \sin\left(\frac{2\pi}{\beta} \cdot \phi\right) = \\ &= \ddot{\varphi} \frac{r_1 - r_2}{\beta} \cdot \left[1 - \cos\left(\frac{2\pi}{\beta} \cdot \phi\right)\right] + \dot{\varphi}^2 \cdot 2\pi \cdot \frac{r_1 - r_2}{\beta^2} \cdot \sin\left(\frac{2\pi}{\beta} \cdot \phi\right) \end{aligned} \tag{9}$$

The calculation of the pressure and flow changes in the chamber between the vanes starts with the determination of the chamber volume and its changes in time. The area between the vanes axis is calculated from /3/:

$$A_{bv}(\varphi) = \frac{1}{2} \cdot \int_0^{\varphi_{n+1}} \rho^2 \cdot d\varphi \; - \frac{1}{2} \cdot \int_0^{\varphi_n} \rho^2 \cdot d\varphi \tag{10}$$

The area of the chamber between the vanes:

$$A(\varphi) = A_{bv}(\varphi) - A_v(\varphi) = A_{bv}(\varphi) - \pi \cdot \frac{s^2}{8} - (\mathrm{r}_{n+1} + r_n - s) \cdot \frac{s}{2} \tag{11}$$

The chamber volume:

$$V(\varphi) = A(\varphi) \cdot b \tag{12}$$

In Fig. 4 the flow balance for the chamber between vanes has been shown /4/.

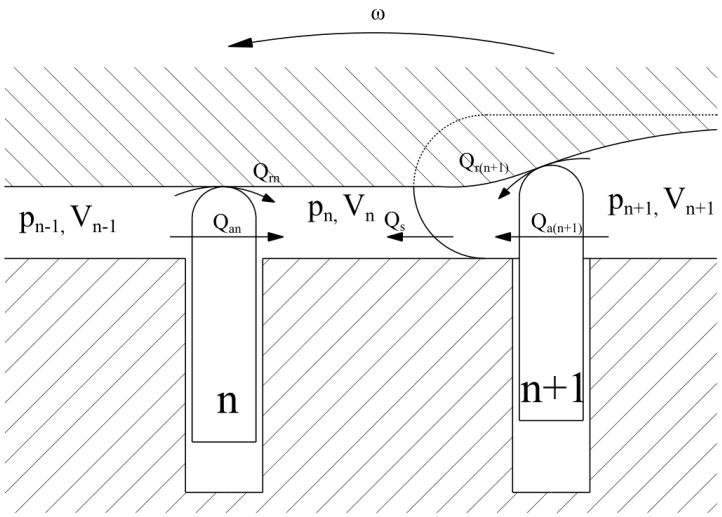

Figure 4: Flow balance inside the chamber between the vanes.

On the basis of the Figure 4 following equation can be written /4/

$Q = Q_a + Q_r + Q_s - Q_z$, where: (13)

Q_a – sum of the flows through axial gaps,

Q_r – sum of the flows through the radial gaps,

Q_s – flow through the kidneys,

Q_z – the change of the chamber volume.

It is assumed a laminar flow through a axial gap in accordance with the formula:

$$Q_{an} = \frac{b \cdot \delta^3}{12 \cdot \mu} \cdot \frac{p_{n-1} - p_n}{l} \cdot \frac{\rho_{f\,0.5(p_{n-1}-p_n)}}{\rho_{f\,0}} \tag{14}$$

The flow through the suction and delivery kidneys:

$$Q_s(\phi) = \alpha_D \cdot A_D(\phi) \cdot \sqrt{\frac{2 \cdot \Delta p}{\rho_f}} \tag{15}$$

The pressure change in the chamber between vanes:

$$dp_z = \frac{dV_z}{k_{sc} \cdot V_z} = \frac{Q \cdot dt}{k_{sc} \cdot V_z} \tag{16}$$

The leakages and the pressure calculations has been performed in the AMESim Program /5/. In Figure 5 the model for calculating the pressure changes has been shown.

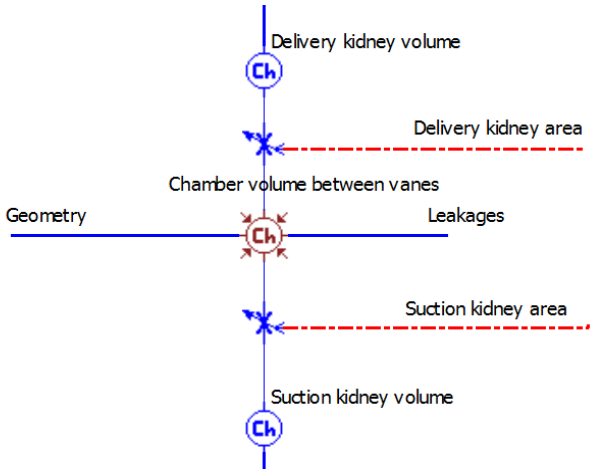

Figure 5: A model for calculating the pressure in the AMESim program.

The suction and delivery kidneys are connected with the chamber volume between the vanes with the throttle valve which represents the variable area between chamber and kidneys. The chamber volume is represented by an element of the variable volume, which is passed to it (along with information about the speed of this change- Q_z) with the features described in MatLab Simulink and transformed to the AMESim . The program also calculates the leaks in the radial and axial gaps. The radial gap is assumed with the constant width and is equal to the width of the vane, while the axial gap varies with the degree of a hanging position of the vanes.

For calculations following data has been defined: $\alpha = 45^0$, $l_0 = 6$ mm, $b = 8$ mm, $s = 1.5$ mm, $f = 0.04$, $\mu = 0.005$.

The pressure changes in the chamber have been shown in Figure 6.

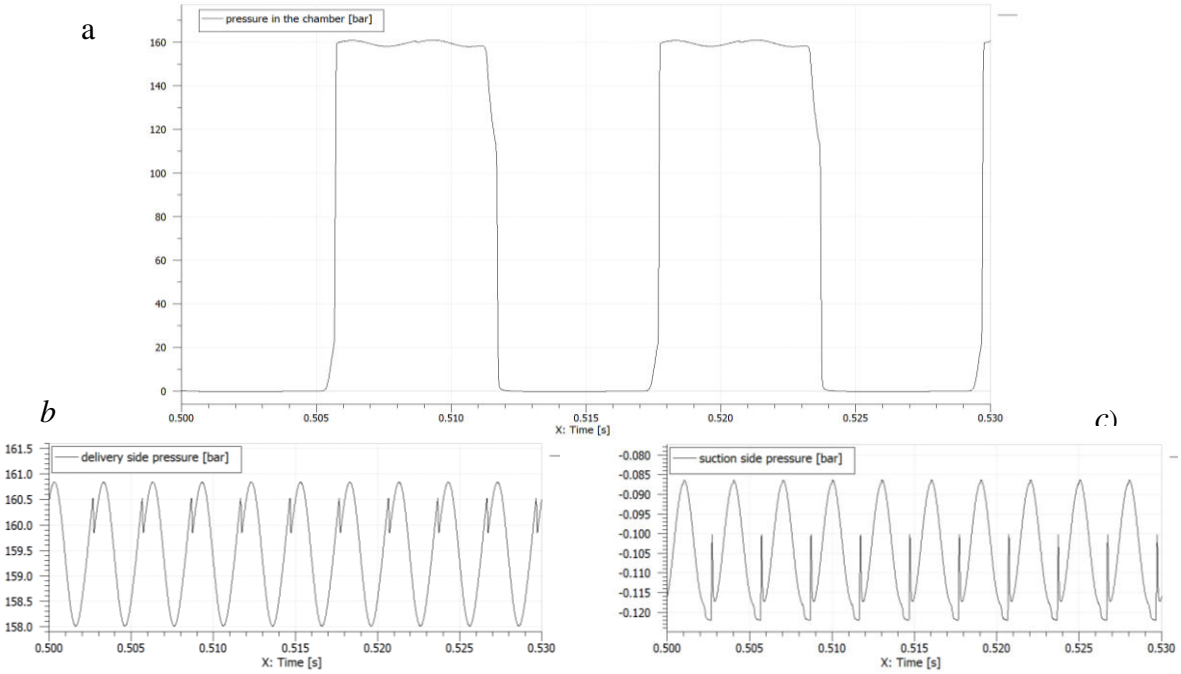

Figure 6: The pressure courses (n=2500 rpm, p = 16 MPa):
a) inside the chamber b) on the delivery side c) on the suction side.

The torque due to the pressure is calculated with the following formula:

$$M_p = -2 \cdot \sum_{n=1}^{z/2} \left[p_n \cdot (r_{n+1} - \rho_n) \cdot b \cdot \frac{r_{n+1} + r_n}{2} \right] = 2 \cdot \sum_{n=1}^{z/2} \left(p_n \cdot \frac{r_n^2 - r_{n+1}^2}{2} \cdot b \right) \tag{17}$$

In order to calculate the torque acting on the pump housing and on the rotor of electric motor, additionally, the torque due to the friction acting on the vanes need to be considered. Schematic view of the forces acting on a single vane is shown in Figure 5. The force F_1 is the sum of the forces of pressure acting on the underside of the vane and the force from the springs:

$$F_1 = F_s + F_p \tag{18}$$

The forces of the F_N, F_2 and F_3 have been determined from Equations (19) to (21) representing the force balance on a single vane.

$$x - axis : F_2 - F_3 + F_N \cdot (\sin\delta - f \cdot \cos\delta) = (p_p - p_l) \cdot l_1 \cdot b \tag{19}$$

$$\begin{aligned} y - axis : & -f \cdot F_2 \cdot sgn(\delta) - F_3 \cdot f \cdot sgn(\delta) + F_N(-\cos\delta - f \cdot \sin\delta) = \\ & = m \cdot \ddot{y} + F_T - F_1 + \frac{s}{2} \cdot b \cdot \left[p_p (1 + \sin\delta) + p_l (1 - \sin\delta) \right] \end{aligned} \tag{20}$$

$$\begin{aligned} M^S : & -F_2 \cdot \left[l_0 + \frac{s}{2} \cdot f \cdot sgn(\delta) \right] + F_3 \cdot \left[l_2 - l_0 + \frac{s}{2} \cdot f \cdot sgn(\delta) \right] - F_N \cdot \frac{s}{2} (\sin\delta\cos\delta) \cdot (f + 1) = \\ & = \frac{b}{2} \cdot (p_l - p_p) \left(l_1^2 + \frac{s^2}{4} \cdot \cos^2\delta \right) \end{aligned} \tag{21}$$

The formula for the moment from reaction forces can be written as:

$$M_T = F_N \cdot r \cdot (f \cdot \cos\delta - \sin\delta) \tag{22}$$

The electric motor load torque:

$$M = M_p + M_T \tag{23}$$

The resulting torque on the pump housing and on the rotor of the electric motor for stationary conditions have been shown in Figure 7.

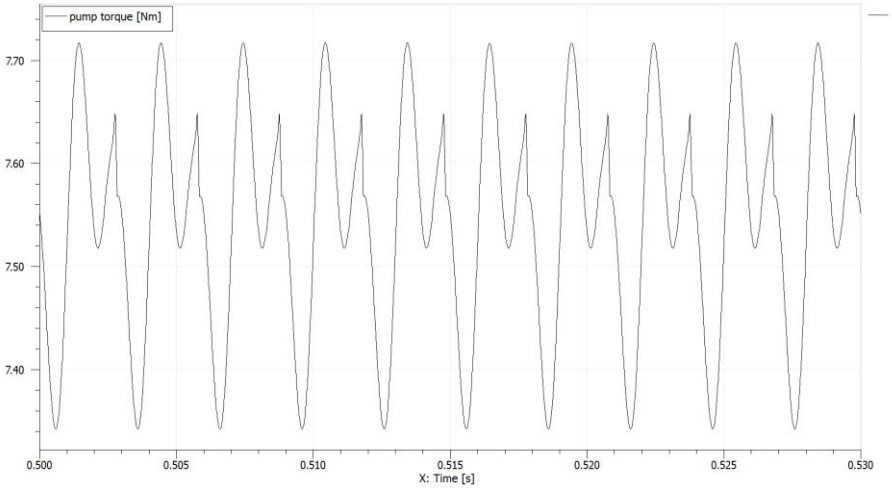

Figure 7: The torque on the pump housing (n = 2500 rpm, p = 16 MPa).

4 Model of the drive system

The pump drive system (Figure 8) consists of the following elements: the supply – control system (power supply and converter with control system with PWM modulator), the BLDC motor with the vane pump and the hydraulic motor. Stabilization of the rotational speed of the hydraulic motor in the drive system has been used (Figure 8). The electric diagram of the converter with a BLDC motor is shown in Figure 9.

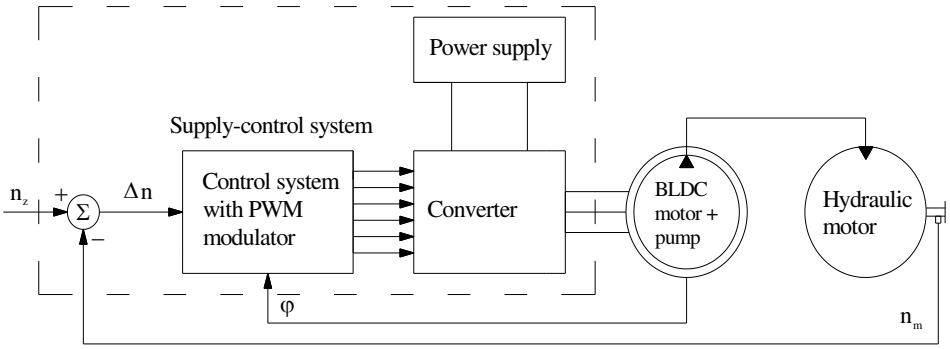

Figure 8: A diagram of the drive system.

Equations (24) – (45) describe the converter – BLDC motor system.

The instantaneous values of the voltages at the motor winding phases *a*, *b* and *c* are as follows (Figure 9)

$$u_a(t,\vartheta) = R(\vartheta)\cdot i_a(t) + \frac{d\psi_a}{dt} = R(\vartheta)\cdot i_a(t) + L\frac{di_a}{dt} + e_a(t) \tag{24a}$$

$$u_b(t,\vartheta) = R(\vartheta)\cdot i_b(t) + \frac{d\psi_b}{dt} = R(\vartheta)\cdot i_b(t) + L\frac{di_b}{dt} + e_b(t) \tag{24b}$$

$$u_c(t,\vartheta) = R(\vartheta)\cdot i_c(t) + \frac{d\psi_c}{dt} = R(\vartheta)\cdot i_c(t) + L\frac{di_c}{dt} + e_c(t) \tag{24c}$$

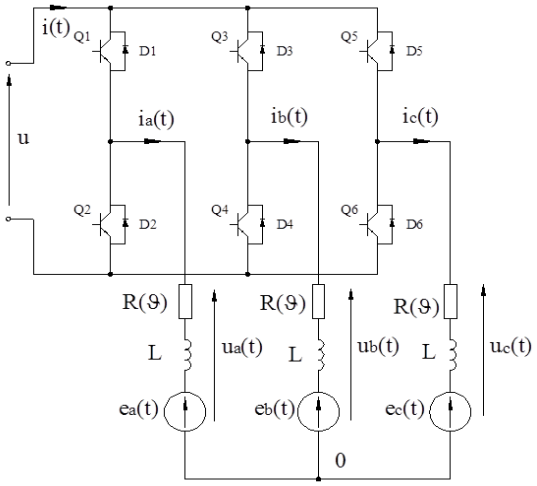

Figure 9: Diagram of the motor with converter.

where: $e_a(t)$, $e_b(t)$, $e_c(t)$ – the instantaneous values of back EMFs induced in the armature winding phases, $R(\vartheta)$- the resistance of the armature winding phases at ϑ temperature, L – the inductance of the one armature winding phase which is the sum of the self inductance and mutual inductance, $i_a(t)$, $i_b(t)$, $i_c(t)$ – the instantaneous values of the currents in the armature windings of *a*, *b* and *c* phases, ψ_a, ψ_b, ψ_c – the instantaneous values of the flux linkage with the armature windings of *a*, *b* and *c* phases.

The equation of currents at 0 node of the system is as follows (Figure 9)

$$i_a(t) + i_b(t) + i_c(t) = 0 \tag{25}$$

while the instantaneous value of the electrical angular speed is calculated as below

$$\omega_e(t) = \frac{d\varphi_e}{dt} = p \cdot \omega(t) \tag{26}$$

where: φ_e – electrical angle of the rotor, p – the number of motor pole pairs, $\omega(t)$ –the instantaneous value of the mechanical angular speed of the motor

$$\omega(t) = \frac{d\varphi}{dt} \tag{27}$$

φ – mechanical angle.

The instantaneous value of back EMF induced in the *k* armature winding phase stems from the presented equations

$$e_k(t) = p \cdot \omega(t) \cdot c_{ek}(\vartheta) \cdot F_{ek}(\varphi_e) = \omega_e(t) \cdot K_{ek}(\varphi_e, \vartheta) \tag{28}$$

$$K_{ek}(\varphi_e, \vartheta) = c_{ek}(\vartheta) \cdot F_{ek}(\varphi_e) \tag{29}$$

where: $c_{ek}(\vartheta)$ –temperature dependent electromotive force constant, $F_{ek}(\varphi_e)$ – function defining the waveform of the back EMF of the *k* phase depending on the electrical φ_e. These functions are shifted for each phase at 120°.

The dependence of the electromotive force as a function of the angle of rotation and motor temperature has been determined through the finite element method.

In the mathematical model of the electrical system all operating states of the converter are taken into account. The different operating states result from conduction of different transistors and diodes of the converter during rotor rotation. The order of transistors and diodes switching on and off is shown in Figure 10.

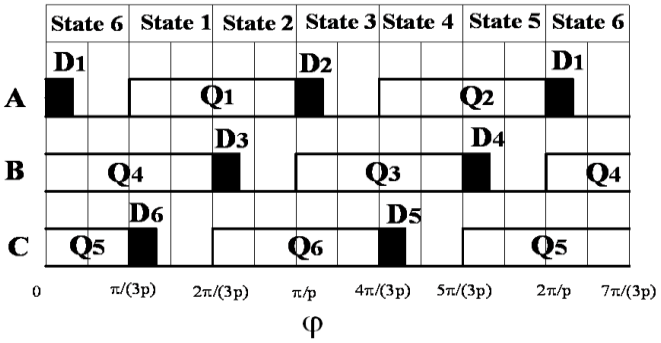

Figure 10: Sequence of switching transistors and diodes of the converter as a function of the mechanical angle.

The time interval in which current of the phase (which is to be disabled) flows through one of the feedback diodes is defined as the commutation interval. At this time, current flows through all the motor winding phases. The conduction interval corresponds to the state in which the current flows only through two supplied phases of the armature winding.

Table 1 shows the current and voltage equations describing the operation of the motor in the first state. In the others motor operating states the equations are analogous /6, 7/.

Commutation interval		**Conduction interval**	
$u_{bc}(t)=\Delta u_d(i_c)-\Delta u_{tr}(i_b)$	(30)		
$u_{ab}(t)=u(t)-\Delta u_{tr}(i_a)+\Delta u_{tr}(i_b)$	(31)	$u_{ab}(t)=u(t)-\Delta u_{tr}(i_a)+\Delta u_{tr}(i_b)$	(36)
$\frac{di_a}{dt}=\frac{1}{3L}\left(\begin{array}{l}2u_{ab}(t)+u_{bc}(t)-2\cdot e_a(t)+e_b(t)+\\+e_c(t)+R\left(-2i_a(t)+i_b(t)+i_c(t)\right)\end{array}\right)$	(32)	$\frac{di_a}{dt}=\frac{1}{2L}\left(\begin{array}{l}u_{ab}(t)-e_a(t)+e_b(t)+\\+R\left(-i_a(t)+i_b(t)\right)\end{array}\right)$	(37)
$\frac{di_b}{dt}=\frac{1}{L}\left(\begin{array}{l}e_a(t)-e_b(t)+R\left(i_a(t)-i_b(t)\right)+\\+L\frac{di_a}{dt}-u_{ab}(t)\end{array}\right)$	(33)	$\frac{di_b}{dt}=-\frac{di_a}{dt}$	(38)
$\frac{di_c}{dt}=-\frac{di_a}{dt}-\frac{di_b}{dt}$	(34)	$\frac{di_c}{dt}=0$	(39)
$i(t)=i_a(t)$	(35)	$i(t)=i_a(t)$	(40)

Table 1. The BLDC motor equations for the first state of the converter operation

In Figure 10 and Table 1, each symbol stands for: $u(t)$ – the instantaneous value of the voltage at the input of the converter, $i(t)$ – the instantaneous value of the converter current drawn from the power supply, *Q1...Q6*– transistors of the converter, *D1...D6* – feedback diodes of the converter, $\Delta u_{tr}(i_k)$– the voltage drop on the converter transistor, $\Delta u_d(i_k)$ - the voltage drop on the converter feedback diode.

The instantaneous value of the electromagnetic torque of the motor equals

$$M_e(t)=p\cdot\sum K_{ek}(\varphi_e,\vartheta)\cdot i_k(t)=p\cdot(K_{ea}(\varphi_e,\vartheta)\cdot i_a(t)+\cdot K_{eb}(\varphi_e,\vartheta)\cdot i_b(t)+K_{ec}(\varphi_e,\vartheta)\cdot i_c(t)) \tag{41}$$

The instantaneous value of the mechanical torque of the motor is

$$M_m(t)=M_e(t)-M_{tm}(t) \tag{42}$$

where: M_{tm} – friction torque of the motor.

The instantaneous value of the motor mechanical power is as follows

$$P_m(t) = M_m(t) \cdot \omega(t) \tag{43}$$

The equation given below describes the drive system torques

$$M_m(t) - M(t) = M_d(t) \tag{44}$$

where: $M(t)$ – load torque generated by the vane pump, $M_d(t)$ – dynamic torque of the electric motor

$$M_d(t) = J\frac{d\omega}{dt} + \frac{\omega}{2}\frac{dJ}{dt} = J\frac{d\omega}{dt} + \frac{\omega^2}{2}\frac{dJ}{d\alpha} \tag{45}$$

J – moment of inertia of the motor.

The model of the drive system developed in the AMESim software is shown in Figure 11.

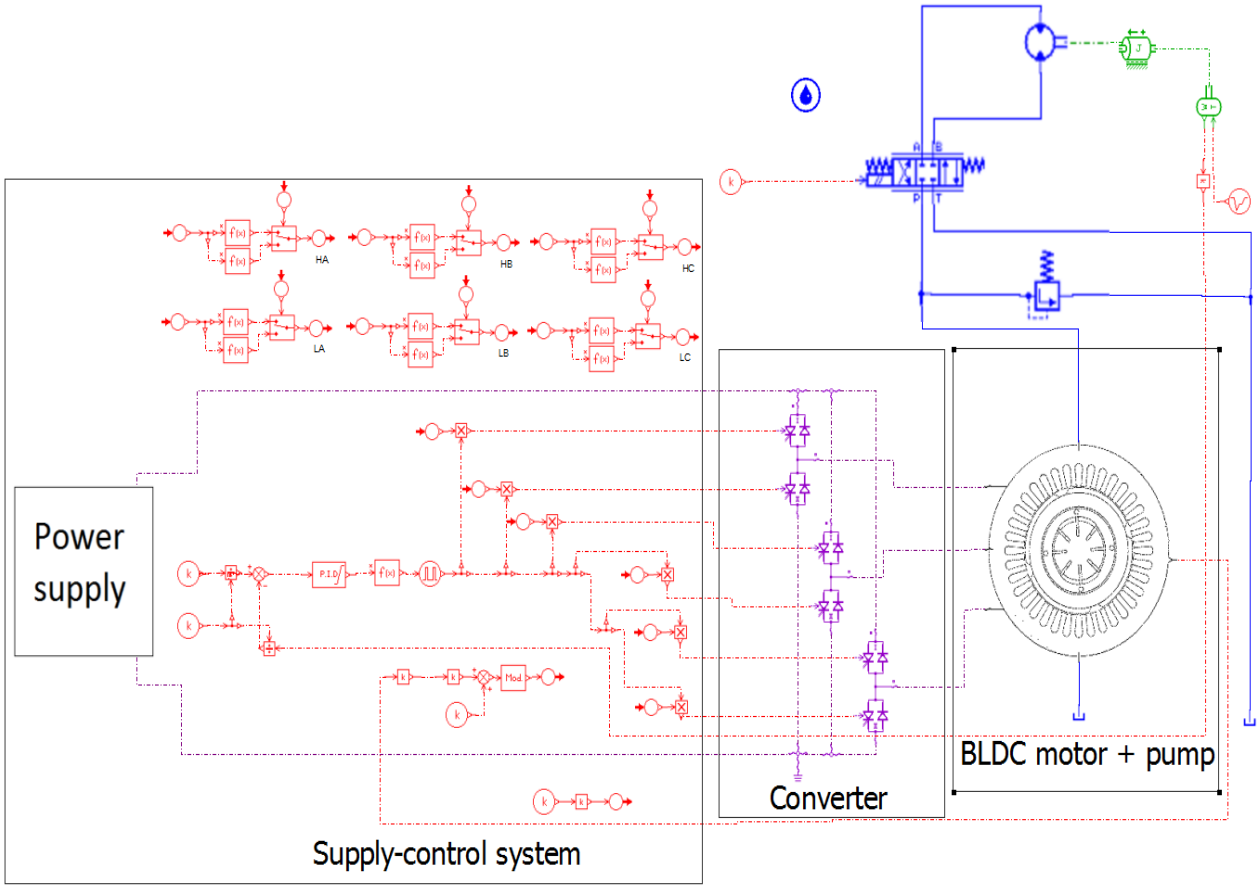

Figure 11: Model of the drive system developed in the AMESim software.

5 Simulation results

In Figure 12 the simulation results has been presented. The response of the drive system to the change (ramp function) of the hydraulic motor torque has been shown. It is clear from the presented results that the changes of the motor torque with the duration time 0.6 s cause relatively small overdue at the beginning and end of the change.

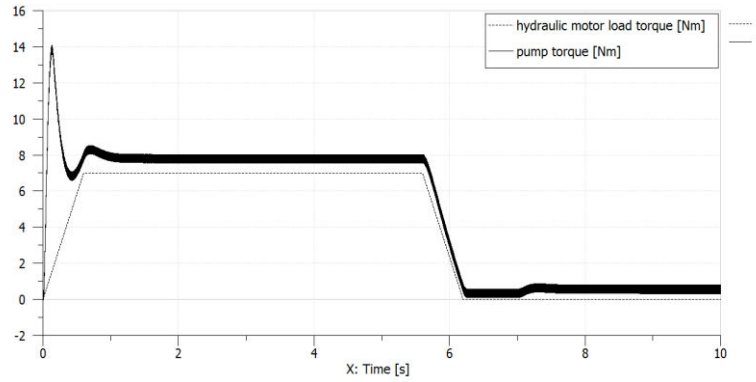

Figure 12: Torque during simulation.

In Figure 13 the diagrams of the rotational speed of the hydraulic motor and of the pump housing, as an answer to the same change of the load torque on the motor (Fig. 12), have been shown.

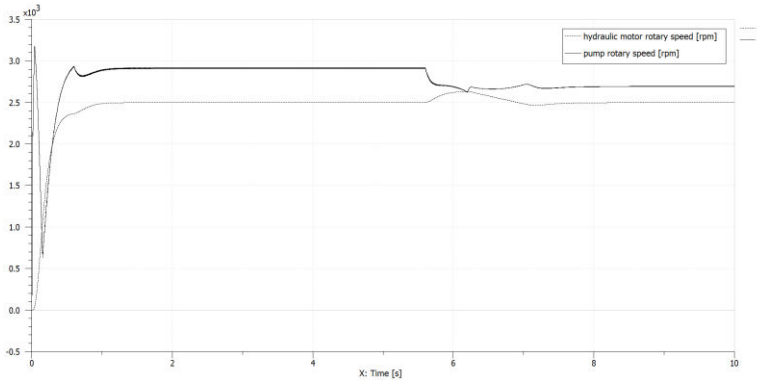

Figure 13: Rotational speed during simulation.

Figure 13 proves that the rotational speed of the hydraulic motor is relatively quickly stabilised after the change of the load torque on the hydraulic motor.

6 Conclusion

The control of the speed of an hydraulic actuator has many advantages, especially regarding energy saving due to the adjustment between the required hydraulic power and the power of the electric motor. The simulation model of the drive system with the BLDC electric motor and the integrated vane pump has been developed. The dynamic load torque of the electric motor has been established on the basis of the analysis of forces due to the pressure acting on the vanes inside the pump. The global model of the drive system contains a description of the dynamic behaviour of the electric motor, the vane pump and the hydraulic motor. With the simulation model the influence of pump parameters as well as the parameters of the electric motor can be analysed to achieve the best dynamic behaviour of the drive system. The results of simulation confirm high dynamic properties of the variable speed drive.

This work has been financed by The Polish National Centre of Research and Development, Project No. 208471.

Nomenclature

Variable	*Description*	*Unit*
ρ_f	Oil density	[kg/m^3]
b	Vane width	[m]
α	Angle between vanes	[rad]
β	Angle of cam ring curve	[rad]
γ	Angle between kidneys	[rad]
ε	Angle between cam ring curves	[rad]
α_D	Discharge coefficient	[-]
A_D	Flow area between kidney and chamber	[m^2]
i	Converter current drawn from the power supply	[A]
i_a, i_b, i_c	Currents in the armature windings of *a*, *b* and *c* phases	[A]
M	Load torque generated by the vane pump	[Nm]
M_e	Electromagnetic torque of the motor	[Nm]
M_m	Mechanical torque of the motor	[Nm]
P_m	Motor mechanical power	[W]
ω	mechanical angular speed of the motor	[rad/s]

References

/1/ Stryczek S. – Hydrostatic drives, WNT, Warsaw1995

/2/ Motor/pump hybrid system EPAI for high and medium- pressure application. Voith Brochure, 2012

/3/ Ivantysyn J., Ivantysynova M - Hydrostatische Pumpen und Motoren. Vogel Verlag Und Druck 1993

/4 Heisel U. , Fiebig W., Matten N. - Druckwechselvorgänge in druckgeregelten Flügelzellenpumpen. Ölhydraulik, Pneumatik 35 (1991)

/5/ Furno F., Vasile L., Andersson D. - The LMS Imagine.Lab AMESim tool for the analysis and the optimization of hydraulic vane pumps. The 11th Scandinavian International Conference on Fluid Power, SICFP09, June 2-4, 2009, Linkoping, Sweden.

/6/ Ciurys, M., Dudzikowski, I., Transients of electrical and mechanical quantities of a brushless DC motor – computations, measurements, In: Archives of Electrical Engineering, vol. 60, nr 1, pp.. 23-34, 2011.

/7/ Dudzikowski, I., Ciurys, M., Commutator and brushless motors excited by permanent magnets, Publishing House of the Wroclaw University of Technology, Wroclaw, 2011 (in Polish).

/8/ Gieras, J., F., Advancements In Electric Machines, Springer , 2008.